ELSEVIER

Image and Vision Computing 16 (1998) 317–327

image AND vision COMPUTING

Euclidean skeletons

Grégoire Malandain*, Sara Fernández-Vidal[1]

INRIA—Project Epidaure, 2004 Route des Lucioles, BP 93, 06902 Sophia Antipolis, Cedex France

Received 17 June 1996; received in revised form 27 October 1997; accepted 30 October 1997

Abstract

An approach for the skeletonization of two-dimensional (2-D) or 3-D objects is presented.

Two local measures, ϕ and d, are introduced to characterize skeleton points in n-D, whose good localization is ensured by Euclidean distance mapping techniques. These measures allow the level of detail in the resulting skeleton to be controlled.

Thresholding these measures does not generally yield a well-defined skeleton: a low threshold preserves the original object's topology but produces a noise sensitive skeleton, while a larger threshold produces a more robust skeleton but it is generally not homotopic with the original object.

To overcome these drawbacks, functions of these measures can be introduced. Although they generally yield convincing experimental results, they are still sensitive to noise. Instead, a novel global step for 2-D and 3-D images called topological reconstruction is introduced, that will provide the skeleton with robustness with respect to noise and ensure homotopy with the original object. Moreover, this method is not iterative (like thinning approaches) and hence has reasonable computational time for 3-D objects. Results on synthetic 2-D patterns and on real 3-D medical objects are presented.

Keywords: skeletonization; distance transform; digital topology

1. Introduction

The skeleton and the medial axis transform (MAT) were introduced to describe the global properties of objects and to reduce the original image to a more compact highly structured representation. In computer vision, this kind of global representation has become increasingly more useful in object identification, recognition, and registration. An important application area for these techniques is medical imaging. Because of significant improvements in medical imaging devices, three-dimensional (3-D) images play an increasingly important role. However, most existing skeletonization approaches were developed for the 2-D case. Even if their theoretical adaptation to the 3-D case does not present any difficulties, their practical implementation may be quite awkward.

To define the skeleton, Blum proposed the grassfire analogy [1]: the skeleton consists of the points where different firefronts intersect, or quench points. Another definition, widely used later, was also introduced by Blum. If one considers the surface obtained from the distance transform of the object, which for each object point gives the distance to the nearest boundary point, the skeleton is the locus of discontinuities of its derivative. In order to formalize the skeleton notion, Calabi analyses the problem from a topological point of view. He gives a skeleton definition based on the concept of maximal disks [2]: the skeleton is the set of the maximal disk centers. He proves that the notions of quench points and centers of maximal disks are equivalent. Similar results are presented by Matheron [3].

Adapting these definitions to the discrete case with an Euclidean metric is extremely difficult. A skeletonization method has to obey the following properties to make its results convenient for the global representation of objects.

- Homotopy: the skeletonization must preserve the topology of the initial object[2].
- Invariance under isometric transformations: the skeleton of a rotated object should be the rotated skeleton.
- Reconstruction: the initial object should be reconstructable from the skeleton.

* Corresponding author. E-mail: Gregoire.Malandain@sophia.inria.fr

[1] Sara Fernandez-Vidal is currently at: Ciencias de la Computacion e Inteligencia Artificial, E.T.S. Ingeniera Informatica, Universidad de Granada, 18071 Granada, Spain.

[2] In 3-D, the object and the skeleton must have the same number of connected components, of holes, and of cavities.

0262-8856/98/$19.00
PII S0262-8856(97)00074-7

In the discrete case, the two last properties will be approximately satisfied.

The 2-D approaches can be classified into four classes: *thinning algorithms* [4–6], *simulations of grassfire propagation* [7], *Voronoï skeletons* [8–10], and *distance transform ridge (or maximal disk center) detection* [11–15]. Each of these previous approaches satisfies some of the desired properties, i.e. thinning algorithms only preserve the topology of the objects, approaches based on distance transform normally ensure the good localization but do not guarantee homotopy of the skeletons and need to be followed by a linking procedure. In general, extending the existing approaches to the 3-D case is impossible or too expensive, due to the use of local patterns or techniques existing only in the 2-D case. One can find an extensive review of the state of the art in a previous publication [16].

We note that the skeleton is known to be enormously sensitive to the smallest change in the boundary of the object [17]. This property becomes a major problem when dealing with digital objects. Most skeletonization techniques use simplification, or *pruning*, to delete part of the skeleton produced by boundary noise.

In this paper, an approach is presented for computing the skeleton of 2-D and 3-D objects, that is twofold.

1. Two parameters, ϕ and d, are introduced for the local characterization of skeleton points. These parameters can be adapted for any dimension and may be combined with other measures to better fit the intuitive notion of skeleton.
2. However, thresholding these parameters or some measure generally does not yield a well-defined skeleton. An original method called topological reconstruction is introduced which will provide the skeleton with robustness with respect to noise and ensure homotopy with the original object.

2. Local characterization of skeleton points in n-D

This characterization is based on Euclidean distance mapping: for each object point, it is assumed that a vector pointing towards its nearest boundary points is known. Efficient algorithms for computing this information already exist [18,19] and can be adapted to any dimension.

A local characterization of skeleton points is proposed based on the examination of these vectors, with no assumption on the dimension of the considered space. For that purpose, two parameters, ϕ and d, are defined which tune the detail level of the skeleton.

2.1. Two measures for local characterization of skeleton points

The Blum definition has been adapted to the discrete case: the skeleton is the locus of the discontinuities of the distance transform derivative. Characterizing such discontinuities, the skeleton points are obtained. A local characterization is made, looking at the distance transform (see Fig. 1). An alternative approach consists of directly finding the centers of the maxima balls [11,20].

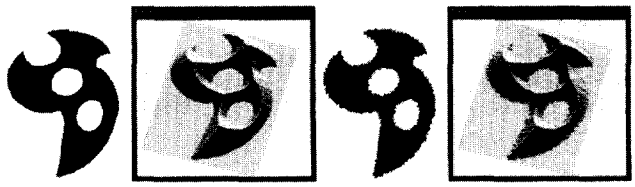

Fig. 1. From left to right: a synthetic 2-D object; the distance transform inside it; the same object with a noisy boundary; the distance transform inside the noisy object. It is clear that the locus of the discontinuities of the distance transform derivative is the skeleton.

Let X be the object to be skeletonized. In an n-dimensional discrete space, X is commonly defined as a finite subset of $\mathbb{Z}^n$. The background of X (or its complement in $\mathbb{Z}^n$) is denoted $\bar{X}$. The distance map of X (inside X) denoted ρ is defined by:

$$\mathbb{Z}^n \rightarrow \mathbb{R}^+$$

$$M \mapsto \rho(M) = d(M, \bar{X}) = \inf_{P \in \bar{X}} d(M, P)$$

where d is a distance function, usually the Euclidean distance (or an approximation of it).

The set of the closest background points of a point M is denoted by $\Pi(M)$. It is defined by:

$$M \mapsto \prod(M) = \{P \in \bar{X} | d(M, P) = \rho(M)\}$$

A point P of $\Pi(M)$ may be computed using Euclidean Distance Transform (EDT) methods [19] (which give the vector $\vec{MP}$): this was called the projection of M[3].

The gradient of the distance map, $\nabla\rho$ may be approximated by $-\vec{MP}$ [16]. This approximation stands in an open neighborhood of M if the distance transform derivative is continuous.

A discontinuity of $\nabla\rho$ about M means that there exists a neighbor M' of M such that its projection, P' (given by $\vec{M'P'}$, output of EDT for point M') is very *different* from P (the projection of M). This *difference* can be measured by either one of the parameters: the angle between $\vec{MP}$ and $\vec{M'P'}$, $\phi = \vec{MP}.\vec{M'P'}$, or the distance $d = \|\vec{PP'}\|$ (see Fig. 2).

Moreover, one checks that M is potentially a maximal ball center. This implies that there exists no neighbor M' of M such that the ball with center M and radius $\|\vec{MP}\|$ is included in the one with center M' and radius $\|\vec{M'P'}\|$. This is equivalent to:

$$\|\vec{MP}\| + \|\vec{MM'}\| \geq \|\vec{M'P'}\| \quad \forall\, M' \text{ neighbor of } M \text{ and } M' \in X. \tag{1}$$

[3] If $\#\Pi(M) \geq 2$, which means that M is the maximal ball center, only one $P \in \Pi(M)$ is given by the EDT.

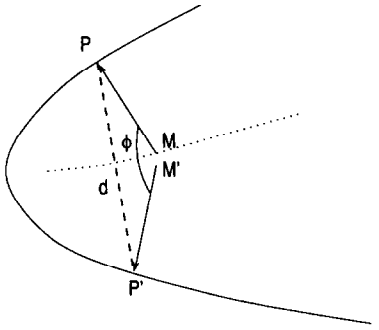

Fig. 2. Definition of the ϕ and d parameters.

In practice one computes:

If $\exists M' \in N(M) \| \|\vec{MP}\| + \|M\vec{M'}P\| \leq \|\vec{M'P'}\|$

else

$$\phi(M) = d(M) = 0$$

$$\begin{cases} \phi(M) = \max\limits_{M' \in N(M)} \left(\widehat{\vec{MP}.\vec{M'P'}}\right) \\ d(M) = \max\limits_{M' \in N(M)} \|\vec{PP'}\| \} \end{cases} \quad (2)$$

where $N(M) = \{N_6^*(M) \cap X\}$ is the set of the 6-neighbors [5] of M belonging to X.

It is obvious that these two parameters are related, since it can easily be established that:

$$\sin\frac{\phi}{2} \approx \frac{d/2}{\|\vec{MP}\|} \text{ assuming } \|\vec{MP}\| \approx \|\vec{M'P'}\| \quad (3)$$

Fig. 3 shows the values of the ϕ and d parameters for the object of Fig. 1, which seem to be sufficient to characterize the skeleton points.

Given a threshold for one of these parameters, the skeleton of an object may be easily computed. The smaller the threshold, the more detailed the skeleton. It must be mentioned that the topology of the resulting skeleton is heavily related to the threshold: a large threshold may result in disconnected skeleton (see Fig. 5).

2.2. Related work

Meyer [17] defines the skeleton using the grassfire analogy: at quench points the firefront speed is greater than one and equal to $1/\sin\beta$, and at points that do not belong to the skeleton, firefronts spread with a speed equal to 1. Using a *β-conditional bisector*, he denotes the set of skeletal points

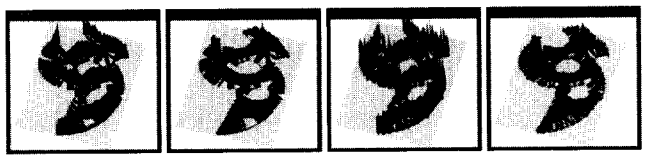

Fig. 3. From left to right: values of ϕ and d for the synthetic object of Figure 1; values of ϕ and d for the noisy synthetic object.

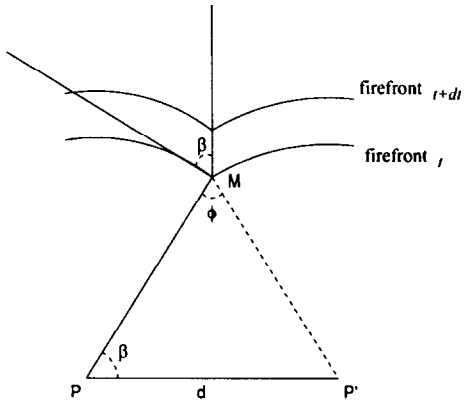

Fig. 4. Definition of β and its relationship with ϕ.

where firefront speed is greater than or equal to $1/\sin\beta$. Fig. 4 shows the relation between ϕ and β angles. More precisely, one has:

$$\pi = 2\beta + \phi$$

In order to obtain the β-conditional bisector of an object, Talbot [14] first computes the value of ϕ for each point of the object, using the distance transform, and then deduces the value of β.

Another angular measure, α, was also introduced by Kruse [21] to define the α-skeleton. α is in fact equal to 2β (as defined by Meyer [17]).

2.3. Reconstruction of the object from its skeleton

The medial axis transform (MAT) is the pair $\{SK(X), \rho_{sk}\}$ where $SK(X)$ denotes the skeleton of X and ρ_{sk} is the restriction of ρ in $SK(X)$. To obtain this pair, one only has to retain, for each pixel M of $SK(X)$, the norm of the vector $\vec{MP}$ (output of EDT for the point M).

The reconstruction of the initial set X is simple, since X is

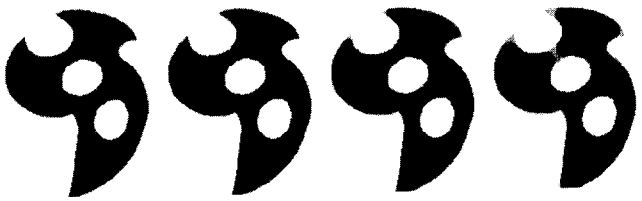

Fig. 5. Skeleton (in black) obtained by thresholding of either ϕ or d, deduced reconstruction (in dark grey), and difference with the original pattern (light grey). From left to right: ϕ is thresholded at 60°; ϕ is thresholded at 120°; d is thresholded at 8 pixels; d is thresholded at 16 pixels.

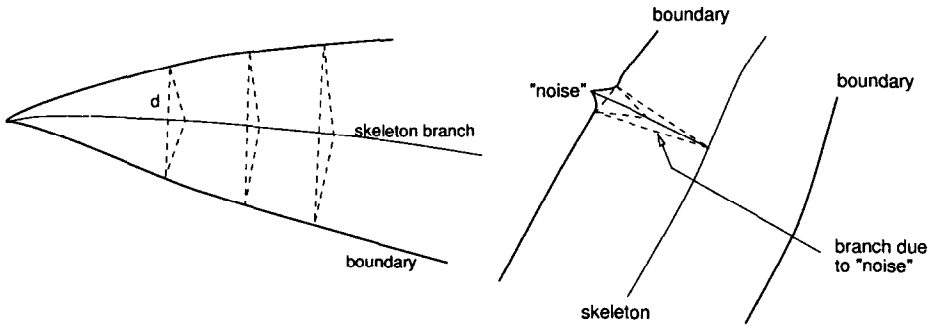

Fig. 6. Different kinds of skeleton branch.

the union of the balls $B_{\rho(M)}(M)$, for all M belonging to $SK(X)$. In Fig. 5, the reconstructed object from skeletons computed by different thresholds of ϕ and d, respectively, is presented.

It is observed that the reconstruction is better for skeletons found with the ϕ parameter than with d.

2.4. Another measure for local characterization of skeleton points

It is obvious (see Figs. 3, and 5) that a simple thresholding of ϕ or d does not ensure all of the desired features for the skeleton. At finer levels, the skeletons are too sensitive to boundary noise; at coarser levels they are disconnected. The skeleton is known to be enormously sensitive to the smallest change in the boundary of the object [17]. This property is a major problem when dealing with the discrete version of objects.

Two types of skeleton branches can be distinguished (see Fig. 6). *Secondary branches* are branches due to noise, or to irrelevant changes in the boundary shape from a global point of view (we are implicitly looking for the shape's global aspect). The rest of the skeleton is the *principal part*, it consists of the skeleton points in the inner part of the object, and the branches coming from significant protrusions of the boundary, which we call *principal branches*. A low threshold of either ϕ or d produces detailed skeletons with many *secondary branches*. As the threshold is increased, some branches of the skeleton disappear: *secondary branches* disappear faster than the *principal branches* which are more robust with respect to parameter change.

Moreover, it is observed that:

- along *secondary branches*, ϕ is rapidly decreasing while d is almost constant (with respect to $\|\vec{MP}\|$)

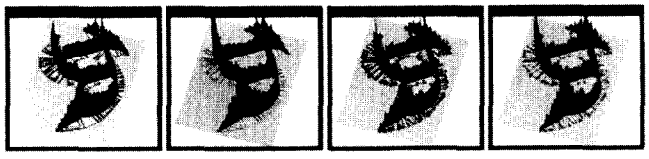

Fig. 7. From left to right: values of functions $f = \phi d$ and $f = \phi d^{3/2}$ for the synthetic object of Figure 1, values of same functions for the noisy synthetic object.

- along *principal branches*, ϕ is decreasing slowly while d increases slowly (with respect to $\|\vec{MP}\|$).

Thus, it may be more interesting to threshold not a single parameter (ϕ or d), but a new measure $f(\phi, d, \|\vec{MP}\|)$ which depends on ϕ, d and $\|\vec{MP}\|$. In fact, a function of only two of these is sufficient as they are related together (see Eq. (3)).

The design of such a function f is not an easy task. We have already tried a condition $d \geq f(\|\vec{MP}\|)$ with encouraging experimental results [22]. Farther experiments have shown that the function $f = \phi d$ where ϕ and d are respectively expressed in degrees and pixels, yields topologically correct results but is still sensitive to noise, although less than a single thresholding of ϕ or d (compare Fig. 3 with Fig. 7). The condition $\phi d \geq 180$ is generally sufficient for most of binary images. Functions $f = \phi^a d^b$ with $(a, b) \in \mathcal{R}_*^{+2}$ allow better performance in the presence of noise, for instance with $(a, b) = (1, 3/2)$.

2.5. The need for a more global step

It has been seen above that designing a measure that will ensure both homotopy with the original object and good robustness with respect to noise is difficult.

On the other hand, it is relatively easy to design a measure which is robust to noise and provides a good reconstruction of the original object (for instance, a large threshold of ϕ, see Fig. 5) or a measure that ensures the homotopy with the original object (a low threshold of d or $\phi d \geq 180$).

To ensure both the homotopy and the robustness of the skeleton, two measures are used: the first one preserves the topology, and the other one tunes the detail level (and avoids sensitivity to local noise). Both of them will be fused in a global step.

3. Topological tools in [2–3]-D

In this section, some topological objects and tools (topological simplification and topological reconstruction) are defined that will be used to carry out the fusion of the two skeletons.

3.1. Thin set

In the continuous world, an object is thin when its dimension is strictly inferior to the dimension of the space in which it is defined. From topology, a thin object is an object with no thickness, or thickness equal to zero, that is to say an object that only contains balls with radius zero.

The skeleton is a thin set (see Meyer [17] for a topology-based proof). What does this mean? It means that between an object and its skeleton, the dimension decreases (as long as the object is not already a thin set). For example, the skeleton of a bidimensional object defined in the 2-D space looks like a graph, composed of pieces of curves. The skeleton of a volume defined in the 3-D space is composed of pieces of surfaces and curves.

Furthermore, it can be said that an object is thin when its skeletonization is the identity transform, that is:

$\mathrm{SK(X)} = \mathrm{X}$ if X is a thin set

$SK(X) = Y, Y$ being a thin set

In the discrete case, everything becomes a little bit more confused. If one wants to preserve the connectivity of the object in a thinning or skeletonization process, the thickness of the result will not be equal to zero everywhere.

To overcome these difficulties, let us consider another way to define a thin object in discrete topology by introducing the concept of a *simple point. A simple point* is a point whose suppression, or addition, does not change the topology of the object. A thin set in an n-D space is an object with no simple points adjacent to a point of a manifold (subset) in dimension n. The simple points adjacent to a point belonging to a manifold of dimension less than or equal to $n - 1$ generally define the stop criterion in the thinning process.

3.2. Topological classification of thin sets in [2–3]-D

The points of a digital object can be classified from a topological point of view. In the 2-D and 3-D spaces, this kind of classification is very interesting when dealing with thin sets.

The topological classification method we are going to use is detailed in Ref. [23]. This classification is based on the local computation of two numbers (see Table 1):

- C^*, number of 26-connected components of $\{X \cap N^*_{26}(x)\}$ 26-adjacent to x,
- $\bar{C}$, number of 6-connected component of $\{\bar{X} \cap N_{18}(x)\}$ 6-adjacent to x,

where X is the digital object to be characterized, $\bar{X}$ its complement, x a point of X. N_{26} is the 26-neighborhood [5] of x. To get $N^*_{26}(x)$, x is removed from N_{26}. $\{X \cap N^*_{26}(x)\}$ is the set of points of X sharing a vertex, an edge, or a face with x. $N_{18}(x)$ is the 18-neighborhood of x. $\{\bar{X} \cap N_{18}(x)\}$ is the set of background points sharing a edge or a face with x.

The use of the 18-neighhorhood to compute $\bar{C}$, instead of the 26-neighborhood, allows us to consider the Type C (frontier points) as *simple points* [24].

There are some deficiencies in this classification, mostly with respect to the junctions. This is due to the fact that the junction thickness of a digital object may not be equal to zero. After this classification, points of Type A may appear in the junctions of several surfaces, or points of Type F may appear in the junctions of several curves. Also some points may be labeled as surface or curve points even though they are junction points.

3.2.1. Pure surfaces and curves in [2–3]-D

Surfaces and curves which do not contain junctions are called pure surfaces and curves. This notion is also introduced in Ref. [23] to solve the problem of badly classified junctions. The skeleton of a tridimensional object comprised almost entirely pure surfaces and curves linked together by junctions.

A pure curve point has only two neighbors and when removed from the curve, the curve is split into two parts ($C^* = 2$). Detecting a badly classified curve point is a trivial matter, one only needs to count the point's neighbors. The pure surface points cannot be detected as easily. To overcome this problem, a pure surface segmentation method is presented in Ref. [23]. A pure surface is a connected component made of points of Type F, which splits its neighborhood background into two connected components.

Let x be a surface point and B_x and C_x be the two connected components of $\bar{X} \cap N_{18}(x)$ 6-adjacent to x. The pure surfaces are the equivalence classes of the following equivalence relation:

Table 1
Topological classification of digital object points according to the values of C^* and $\bar{C}$

Type A	Volume point	$\bar{C} = 0$	
Type B	Isolated point		$C^* = 0$
Type C	Frontier point	$\bar{C} = 1$	$C^* = 1$
Type D	Curve point	$\bar{C} = 1$	$C^* = 2$
Type E	Curve junction point	$\bar{C} = 1$	$C^* > 2$
Type F	Surface point	$\bar{C} = 2$	$C^* = 1$
Type G	Surface–curve(s) junction point	$\bar{C} = 2$	$C^* \geq 2$
Type H	Surfaces junction point	$\bar{C} > 2$	$C^* = 1$
Type I	Surfaces–curve(s) junction point	$\bar{C} > 2$	$C^* \geq 2$

Table 2
Using the 26-connectivity to extract pure surfaces of the synthetic object of Fig. 8

Using the 26-connectivity to segment the pure surfaces

Number of frontier points	716
Number of surface points	21222
Number of junction points	2406

Extraction of pure surfaces

Label of the surface	Number of points	Label of the surface	Number of points
1	2856	7	314
2	2744	8	666
3	1972	9	1370
4	2009	10	412
5	1976	11	3268
6	3042	12	593

Extraction of the junctions

Label of the junction	Number of points	Label of the junction	Number of points
1	580	4	312
2	525	5	340
3	424	6	225

Two points x, y of Type F are in relation (they belong to the same pure surface) if and only if there is a 26-path $x_0, x_1, \ldots, x_n$ of Type F points, where $x_0 = x$ and $x_n = y$, $0 \leq i \leq n$, such that one of the following two conditions holds:

- $B_{x_i} \cap B_{x_{i+1}} \neq 0$ and $C_{x_i} \cap C_{x_{i+1}} \neq 0$
- $B_{x_i} \cap C_{x_{i+1}} \neq 0$ and $C_{x_i} \cap B_{x_{i+1}} \neq 0$

Thus the badly classified surface points are detected in the following way: it is only necessary to check for each surface point, using between its 26-neighbors those that are also surface points, that there are not several pure surfaces in a $5 \times 5 \times 5$-neighborhood. That is to apply the last relation in a $5 \times 5 \times 5$-neighhorhood and not in all the image.

After the classification process, a thin object will be composed of three kinds of connected components: pure surfaces (or curves), junctions, and frontiers.

In Ref. [23], the 26-connectivity is used as the path between two points of the surface. Because a pure surface is a 26-connected component but also a 18-connected component, the 18-connectivity was used to get paths to find the surface junction points badly labeled as surface points.

In Table 2 and Table 3, results are given of the classification of the synthetic object of Fig. 8. The results of the

Table 3
Using the 18-connectivity to extract pure surfaces of the synthetic object of Fig. 8. The numbering of the components (pure surfaces or junctions) is the same as the numbering in the Table 2

Using the 18-connectivity to segment the pure surfaces

Number of frontier points	716
Number of surface points	21692
Number of junction points	1936

Extraction of pure surfaces

Label of the surface	Number of points	Label of the surface	Number of points
1	2888	7	316
2	2780	8	676
3	2048	9	1406
4	2049	10	440
5	2094	11	3264
6	3134	12	597

Extraction of the junctions

Label of the junction	Number of points	Label of the junction	Number of points
1	512	4	293
2	279	5	348
3	340	6	164

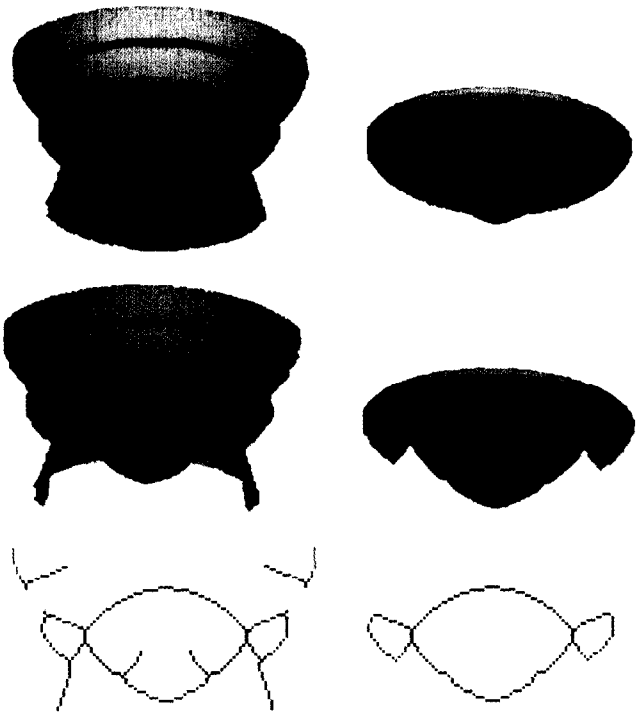

Fig. 8. Topological simplification of a 3-D object.

classification using 26-connectivity or 18-connectivity are identical in a qualitative sense (we obtained the same number of pure surfaces and junctions), but the results using 18-connectivity are more interesting in a quantitative sense because the junctions are thinner (they are composed of less points) and the pure surfaces are larger (they are composed of more points).

3.2.2. Why not in n-D?

In the previous sections, a topological classification was introduced based on two numbers, $\bar{C}$ and C^*. Although a tridimensional formalism was used, they may be easily defined in n-D. However, a complete topological classification, based on only those two numbers, cannot be established in n-D. The explanation lies in their significance.

On the one hand, $\bar{C} = 2$ means that the background is locally divided into two parts, or that the foreground is locally homotopic to a $(n\text{-}1)$-manifold. On the other hand, $C^* = 2$ means that the foreground is locally homotopic to a 1-manifold (a curve).

As the topological characterization of both 0- and n-manifolds is straightforward ($C^* = 0$ and $\bar{C} = 0$), we are able to characterize 0-, 1-, $(n-1)$- and n-manifolds with only those two numbers, but not the i-manifolds, with $1 < i(n-1$, which are considered as made of *frontier points* (see Table 1); this will lead to inconsistent results.

Thus, the above classification and what follows can only be applied in 2- or 3-D.

3.2.3. Simple surfaces and curves

The notion of *simple point* is to be extended to a higher level: the connected components. It has been seen that the removal of a object's simple point does not change the topology of the object. A *simple connected component* will be defined as a pure component (a surface or a curve) such that its removal does not change the topology of the object.

We consider that a pure surface/curve is a simple connected component if it is in contact with only one frontier component. It is clear that when one, or several, simple connected components are removed from an object, the status of other pure components of the object may change and then simple connected components may appear again.

3.3. Topological simplification in [2–3]-D

The topological simplification operation is defined as the removal of the simple connected components of an object. This is a thinning method where *simple connected components* (instead of *simple points*) are iteratively deleted. The following algorithm finds and removes all the simple connected components of a thin object:

1. Topological classification of the object.
2. Labeling of the frontier connected components. If the number of frontiers is zero: the simplification is terminated.
3. Labeling of the pure surfaces/curves.
4. Removal of all the simple surfaces/curves and the frontiers involved with them.
5. Go back to 1.

The effects of this process applied to a 3-D thin object can be seen in Fig. 8 (on the left, the initial object and on the right, the final result of the simplification process). It can be observed that the object has been simplified a lot but still keeps the same topology.

3.4. Topological reconstruction

The reconstruction of an image Y with respect to another image X is a well-known process in image processing. This operation can be defined in this way: let X and Y be two binary images (X and Y also reference the objects in the images). The reconstruction of Y (usually called the marker image) with respect to X consists of keeping the connected components of X having at least one point belonging to Y. This operation allows one to extract some regions of X that contain known interesting regions (connected components of Y or markers).

The topological reconstruction process follows the same idea. Let X be an object with a given topology, and let Y be some parts of X. The topological reconstruction of Y with respect to X consist in adding to Y some parts of $X \backslash Y$ to make Y homotopic to X. This operation can be formalized in the following way: find a subset Z of X such

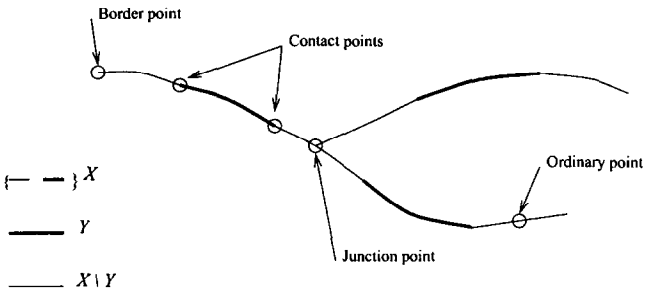

Fig. 9. Labeling of X/Y.

that:

$$Z \cap Y = 0$$

$$\text{topology}(Z \cap Y) = \text{topology}(X)$$

It is clear that one is looking for (one of) the smaller subset Z verifying these conditions. In this context, dealing with thin sets, this operation can also be described as the removal of the connected components of $X\backslash Y$ that does not change the topology of X. Thus, a process has been designed for the construction of Z which is quite simple and very similar to the topological simplification.

1. Topological characterization of $X\backslash Y$. A point of $X\backslash Y$ will belong to one of the three classes: frontier (Type C), *junction* (Types E, G, H, I), *pure surface/curve* (Types D, F).
2. Label change: a new class of points, the contact points, is introduced, which are points of X neighbors of the set Y. Thus some $X\backslash Y$ point labels will be changed, mostly for the points belonging to the frontier class (see the Fig. 9).
3. Topological simplification of $X\backslash Y$: The connected components in contact with only one frontier component will be deleted iteratively. The contact points are indeed considered as pure surface or curve points. This final step provides the subset Z.

Four examples of topological reconstruction are given in Fig. 10. For each example, the left part represents a graph structure, where black parts (also labeled with an asterisk) are parts of Y and the rest of the graph belongs to X. At the right of each picture, one can see the results of the topological reconstruction.

4. The global fusion step

The principle of this step is to combine information coming from two skeletons. A first skeleton, denoted by SK_M, will give the detail level of the skeleton, i.e. the important parts to be preserved. A second skeleton, denoted by SK_m, will give the topology to be preserved. It is assumed that SK_m and the initial object are homotopic and that $SK_M \subset SK_m$ (which can always be ensured by considering $\{SK_M \cup SK_m\}$ as SK_m). As SK_m may indeed have too many branches which are not significant, we want to extract from SK_m only the parts that are relevant in a topological sense. This is the same as removing parts of SK_m/SK_M without changing the topology of SK_m, in other words the topological reconstruction of SK_M with respect to SK_m. This is achieved in two steps

1. Thinning of $SK_m\backslash SK_M$. The thinning method that was used consists of the detection and deletion of simple points, that is, points whose removal does not change the topology of the set SK_m. The resulting set is TSK_m.

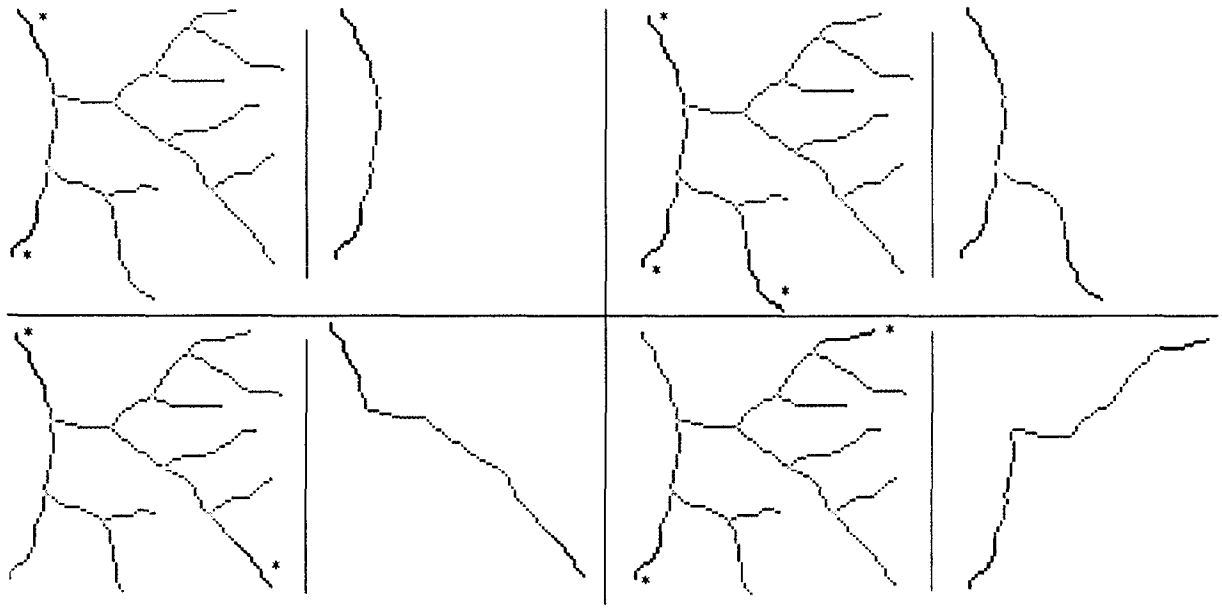

Fig. 10. Four examples of topogical reconstruction. In each picture, there is: left, a graph structure (the skeleton) where black parts (also labeled with an asterisk) are parts of SK_M, the rest being SK_m; right, the result of the topogical reconstruction of SK_M with respect to SK_m.

2. Topogical reconstruction of SK_M with respect to TSK_m as detailed in Section 3.4.

In contrast to the local characterizations of skeleton points presented before, this topological reconstruction can only be applied for objects in a 2- or 3-D space.

4.1. The choice of SK_M and SK_m

SK_M has to be chosen to set the wanted detail level of the final skeleton. SK_m has to be chosen to set the homotopy of the final skeleton. Ideally, it has to be homotopic to the original object, which is not proven here. However, our practical choices of SK_m verify this property.

To be fair, the choice of SK_M and SK_m should be context dependent. However, this context (quality of the images) does not change for a given practical application; as a consequence, both SK_M and SK_m are quite easy to choose.

It was observed that for most images (smooth and few noise patterns) a large threshold of ϕ gives a robust skeleton which allows the original object to be reconstructed (see Fig. 5). Moreover for these images, the condition $\phi d \geq 180$ seems sufficient to ensure the homotopy with the object to be skeletonized (see Fig. 11).

However, for really noisy images as the one presented in Fig. 1, large values of ϕ may be obtained near the boundary. For this reason, it is better to threshold d and use a threshold larger than 180 for ϕd.

For our practical applications, we choose SK_M and SK_m as follows:

> SK_M is defined practically by $\{M$ such that $\phi \geq \phi_{\min}\}$ where the threshold $\phi_{\min}$ is chosen quite large (about 90°).
> SK_m is defined by $\{M$ such that $(\phi d \geq 180$ OR $\phi \geq \phi_{\min})\}$ where the second part of the definition ensures that we have $SK_M \subset SK_m$.

These definitions of SK_M and SK_m require the tuning of a single threshold, $\phi_{\min}$. Moreover, SK_M and SK_m are not very sensitive to this choice, assuming that $\phi_{\min}$ is chosen to be quite large.

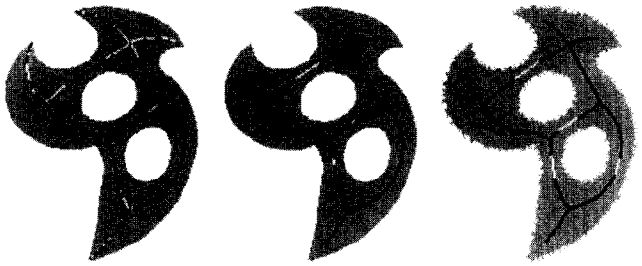

Fig. 11. From left to right: skeleton of the synthetic object of Figure 1 with $SK_m = \{\phi \geq 120\}$ and $SK_M = \{\phi d \geq 180\}$; skeleton of the same object, with $SK_m = \{d \geq 16\}$ and $SK_M = \{\phi d \geq 180\}$ skeleton of the noisy object of Figure 1, with $SK_m = \{d \geq 16\}$ and $SK_M = \{\phi d \geq 360\}$. For the three figures, SK_m is black while parts due to the topological reconstruction with SK_M are white.

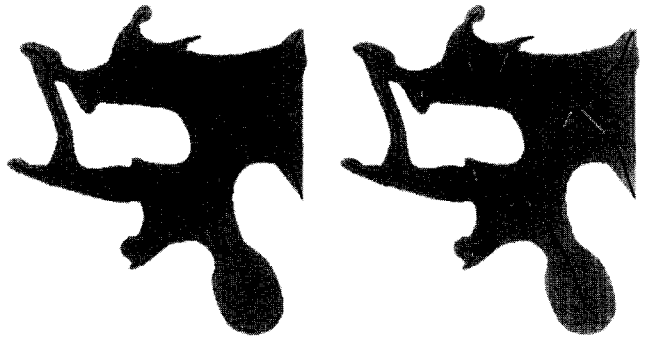

Fig. 12. Left, skeleton found with a threshold $\phi \geq 100°$. Right, skeleton found with our method ($SK_m = \{\phi \geq 100\}$, $SK_M = \{\phi d \geq 180\}$): SK_m is black while parts due to the topological reconstruction with SK_M are white.

5. Results

Our method was applied to different 2-D synthetic objects and following results were obtained.

In Figs 12 and 13, skeletons extracted from synthetic objects are shown. On the left of Fig. 12, one can see the skeleton (in black) extracted by thresholding ϕ with some large threshold, superimposed on the original object (in grey). This skeleton is not homotopic with the original object. On the right of the same figure is shown the perfectly connected skeleton obtained with our method.

Fig. 13 presents the skeletons computed on two occurrences of another pattern, one being rotated with respect to the other. It was observed that the same thresholding of ϕ does not result in the same skeleton (see the black parts). With our approach, similar skeletons are obtained.

The same method was applied to real 3-D objects obtained from 3-D medical images. First a vertebra is processed which was obtained in a 3-D X-ray CT image, containing about $256 \times 256 \times 50$ voxels (each voxel is $0.5 \times 0.5 \times 1$ mm^3) whose intensity is coded with 256 discrete values. This image was resampled to obtain isotropic voxels. A 3-D representation of the vertebra is shown on the left of Fig. 14. The corresponding skeleton is shown on the right of the same figure.

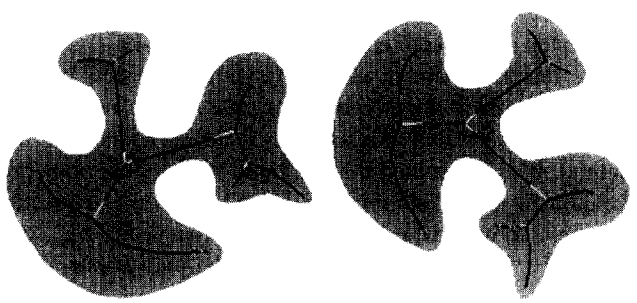

Fig. 13. Left, skeleton computed on a binary pattern ($SK_m = \{\phi \geq 100\}$, $SK_M = \{\phi d \geq 180\}$). Right, skeleton computed with the same parameters on the rotated pattern (30°).

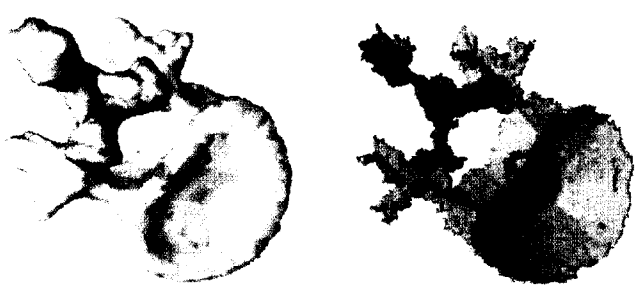

Fig. 14. Left, a 3-D representation of the vertebra. Right, its skeleton obtained with the presented method ($\phi_{min} = 90°$).

One interesting application of our skeletonization method is the automatic extraction of sulci[4]. The top row of Fig. 15 shows three orthogonal slices of a 3-D MR image of the brain. From this data set, first the negative mould of the cortex is segmented to include part of the grey matter. Second, its skeleton is computed (see Fig. 15). A 3-D representation of the brain with its sulci (characterized as being the junctions between surfaces in the skeleton [23]) is presented in Fig. 16.

6. Conclusion

A skeletonization algorithm driven by Euclidean distance mapping has been described. This feature guarantees the invariance under isometric transformation of the results.

First, two local measures, ϕ and d, were presented, which may be combined into more complex functions $f(\phi, d)$, which allow the skeleton to be computed for n-dimensional objects. Finding the *appropriate* function f is not an easy task and we indicate how to distinguish between main and secondary branches, using the two previous measures. It must be pointed out that this distinction should be context dependent.

Thresholding these local measures does not ensure the homotopy of the obtained skeleton with the original object, or its robustness with respect to noise. Thus, a global step, called topological reconstruction, was introduced, which provides the skeleton with the two above properties. Its principle is to fuse information coming from two skeletons: the first one provides the topology to be preserved while the second one specifies the desired detail level of the final skeleton. This global step can be applied either in 2-D or in 3-D.

The results obtained with 2-D synthetic objects or 3-D real objects prove the effectiveness of the proposed method.

The choice of both SK_M and SK_m is the cornerstone of the method. It was assumed that SK_m and the original object to skeletonize are homotopic, or that SK_m has the requested topology. It would be better to prove that some SK_m can be found with this property. This will be part of our future work.

[4] A sulcus (plural sulci) is a shallow furrow on the surface of the brain separating adjacent convolutions.

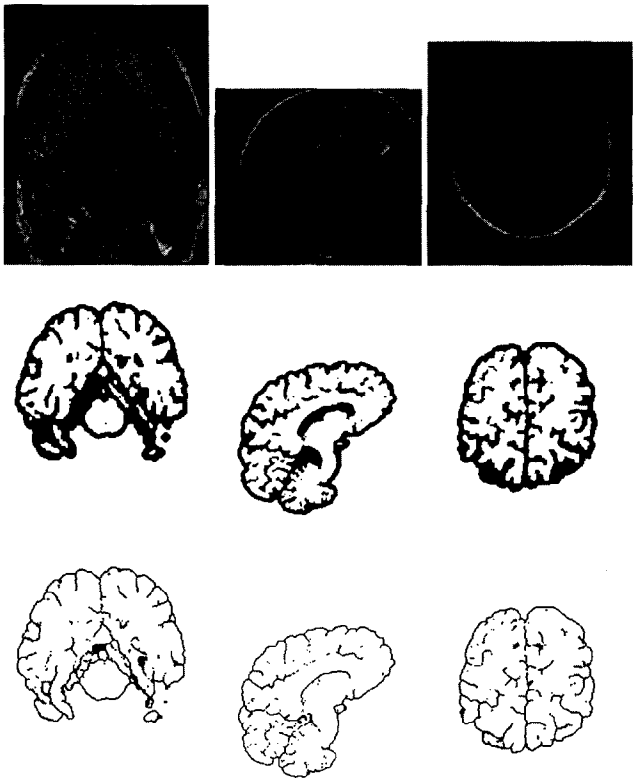

Fig. 15. Top row: three orthogonal slices of a 3-D MR image of the brain. Middle row: the negative mould of the cortex in the same slices. Bottom row: the 3-D skeleton of the negative mould of the cortex.

Acknowledgements

Vertebra data is courtesy of Dr Jean-Louis Coatrieux of INSERM U355 Laboratory, Rennes, France. MR data was provided by Dr Neil Roberts of the Magnetic Resonance and Image Analysis Research Centre, Liverpool University, UK.

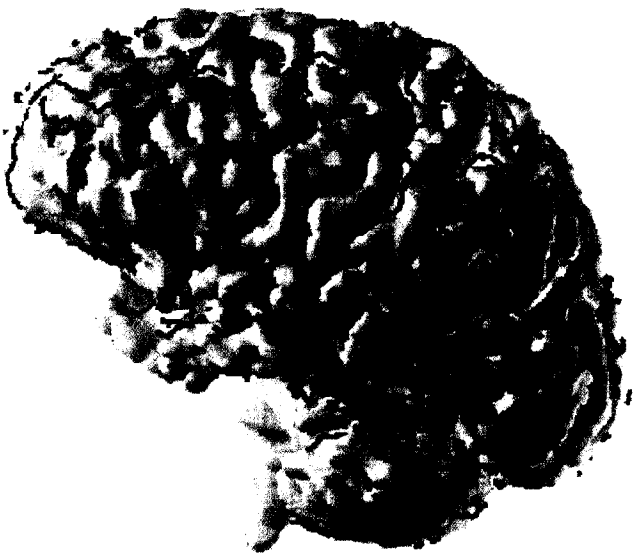

Fig. 16. 3-D representation of the brain and the sulci.

Many thanks are due to Dr Janet Bertot for her help in preparing this article. We would also like to thank the reviewers for their constructive comments.

References

[1] H. Blum, A transformation for extracting new descriptors of shape, in: W. Wathen-Dunn (Ed.), Models for the Perception of Speech and visual Form, MIT Press, Cambridge, MA, 1967, pp. 362–380.

[2] L. Calabi, A study of the skeleton of plane figures, Technical Report 60429, sr-2, Parke Mathematical Laboratories, December 1965.

[3] G. Matheron, Image Analyse and Mathematical Morphology, Vol. 2, Jean Serra, Academic Press, 1988, Chapters 11 and 12, pp. 217–256.

[4] W.X. Gong and G. Bertrand, A simple parallel 3-D thinning algorithm, in: *10th International Conference on Pattern Recognition*, Atlantic City, 17–21 June 1990.

[5] T.Y. Kong, A. Rosenfeld, Digital topology: introduction and survey, Computer Vision, Graphics, and Image Processing 48 (1989) 357–393.

[6] Y.F. Tsao, K.S. Fu, A 3-D parallel skeletonization thinning algorithm, IEEE PRIP Conference, 1982, pp. 678–683.

[7] I. Xia, Skeletonization via the realisation of the fire front's propagation and extinction in digital binary shapes, IEEE Transactions on Pattern Analysis and Machine Intelligence 11 (10) (1989) 1076–1086.

[8] D. Lee, Medial axis transformation of a planar shape, IEEE Transactions on Pattern Analysis and Machine Intelligence 4 (1982) 363–369.

[9] J.W. Brandt, Describing a solid with the three-dimensional skeleton, in: Curves and Surfaces in Computer Vision and Graphics 111, Vol. 1830, SPIE, 1992, pp. 258–269.

[10] R.L. Ogniewicz, Skeleton-space: a multiscale shape description combining region and boundary information, in: Computer Vision and Pattern. Recognition (CVPR '91), IEEE, Seattle, USA, June 1994, pp. 746–751.

[11] F. Meyer, Digital euclidean skeleton, in: Visual Communication and Image Processing volume 1360, SPIE, Lausanne, Switzerland, 1990, pp. 251–262.

[12] C. Arcelli, G. Sanniti di Baja, Ridge points in Euclidean distance maps, Pattern Recognition Letters 13 (4) (1992) 237–243.

[13] C.W. Niblack, P.B. Gibbons, D.W. Capson, Generating skeletons and centerlines from the distance transform, Computer Vision, Graphics, and Image Processing 54 (5) (1992) 420–437.

[14] H. Talbot, L. Vincent, Euclidean skeletons and conditional dissectors, in: Visual Communications and Image Processing, Vol. 1818, SPIE, 1992, pp. 862–876.

[15] C. Arcelli, G. Sanniti di Baja, Euclidean skeleton via centre-of-maximal-disc extraction, Image and Vision Computing 11 (3) (1993) 163–173.

[16] S. Fernández-Vidal, G. Malandain, Squelettes euclidiens d'objets discrets n-dimensionnels, Technical Report 2771, INRIA, 2004 route des Lucioles BP 93, 06902 Sophia Antipolis Cedex, France, janvier 1996.

[17] F. Meyer, Cytologie quantitative et morphologic Mathematique, PhD thesis, École des Mines, May 1979.

[18] P.E. Danielsson, Euclidean distance mapping, Computer Graphics and Image Processing 14 (1980) 227–248.

[19] I. Ragnemalm, The euclidean distance transform in arbitrary dimensions, Pattern Recognition Letters 14 (11) (1993) 883–888.

[20] G. Borgefors, I. Ragnemalm, G. Sanniti di Baja, The euclidean distance transform: finding the local maxima and reconstructing the shape, in: 7th Scandinavian Conference on Image Analysis (SCIA '91), 1991, pp. 974–981.

[21] B. Kruse, An exact sequential euclidean distance algorithm with application to skeletonizing, in: 7th Scandinavian Conference on Image Analysis (SCIA '91), pp. 982–992, 1991.

[22] S. Fernández-Vidal, G. Malandain, Digital euclidean skeleton in n-D, in: 9th Scandinavian Conference on Image Analysis (SCIA '95), IAPR, Uppsala, Sweden, 6–9 June 1995, pp. 517–524.

[23] G. Malandain, G. Bertrand, N. Ayache, Topological segmentation of discrete surfaces, International Journal of Computer Vision 10 (2) (1993) 183–197.

[24] G. Bertrand, G. Malandain, A new characterization of three-dimensions simple points, Pattern Recognition Letters 15 (2) (1994) 169–175.